Measurements of Branching Fraction, Polarization, and Direct-CP-Violating Charge Asymmetry in $B^+ \rightarrow K^{*0}\rho^+$ Decays

The BABAR Collaboration

August 18, 2004

Abstract

With a sample of 88.8×10^6 $B\bar{B}$ pairs produced at PEP-II in e^+e^- annihilation through the $\Upsilon(4S)$ resonance and recorded with the BABAR detector, we search for the $B^+ \rightarrow K^{*0}\rho^+$ decay mode. A signal is observed for the first time with a significance of more than 5σ. We measure a preliminary branching fraction of $\mathcal{B}(B^+ \rightarrow K^{*0}\rho^+) = [17.0 \pm 2.9(\text{stat}) \pm 2.0(\text{syst})^{+0.0}_{-1.9}(\text{non-resonant})] \times 10^{-6}$. The "non-resonant" error corresponds to the uncertainty from non-resonant backgrounds not modeled in the fit. The measurement of the longitudinal-polarized component to this vector-vector penguin decay is of special interest. We measure $f_L = 0.79 \pm 0.08(\text{stat}) \pm 0.04(\text{syst}) \pm 0.02(\text{non-resonant})$. We measure the direct-CP-violating charge asymmetry in this mode to be $\mathcal{A}_{CP} = -0.14 \pm 0.17(\text{stat}) \pm 0.04(\text{syst})$.

Submitted to the 32$^{\text{nd}}$ International Conference on High-Energy Physics, ICHEP 04,
16 August—22 August 2004, Beijing, China

The *BABAR* Collaboration,

B. Aubert, R. Barate, D. Boutigny, F. Couderc, J.-M. Gaillard, A. Hicheur, Y. Karyotakis,
J. P. Lees, V. Tisserand, A. Zghiche

Laboratoire de Physique des Particules, F-74941 Annecy-le-Vieux, France

A. Palano, A. Pompili

Università di Bari, Dipartimento di Fisica and INFN, I-70126 Bari, Italy

J. C. Chen, N. D. Qi, G. Rong, P. Wang, Y. S. Zhu

Institute of High Energy Physics, Beijing 100039, China

G. Eigen, I. Ofte, B. Stugu

University of Bergen, Inst. of Physics, N-5007 Bergen, Norway

G. S. Abrams, A. W. Borgland, A. B. Breon, D. N. Brown, J. Button-Shafer, R. N. Cahn,
E. Charles, C. T. Day, M. S. Gill, A. V. Gritsan, Y. Groysman, R. G. Jacobsen, R. W. Kadel,
J. Kadyk, L. T. Kerth, Yu. G. Kolomensky, G. Kukartsev, G. Lynch, L. M. Mir, P. J. Oddone,
T. J. Orimoto, M. Pripstein, N. A. Roe, M. T. Ronan, V. G. Shelkov, W. A. Wenzel

Lawrence Berkeley National Laboratory and University of California, Berkeley, CA 94720, USA

M. Barrett, K. E. Ford, T. J. Harrison, A. J. Hart, C. M. Hawkes, S. E. Morgan, A. T. Watson

University of Birmingham, Birmingham, B15 2TT, United Kingdom

M. Fritsch, K. Goetzen, T. Held, H. Koch, B. Lewandowski, M. Pelizaeus, M. Steinke

Ruhr Universität Bochum, Institut für Experimentalphysik 1, D-44780 Bochum, Germany

J. T. Boyd, N. Chevalier, W. N. Cottingham, M. P. Kelly, T. E. Latham, F. F. Wilson

University of Bristol, Bristol BS8 1TL, United Kingdom

T. Cuhadar-Donszelmann, C. Hearty, N. S. Knecht, T. S. Mattison, J. A. McKenna, D. Thiessen

University of British Columbia, Vancouver, BC, Canada V6T 1Z1

A. Khan, P. Kyberd, L. Teodorescu

Brunel University, Uxbridge, Middlesex UB8 3PH, United Kingdom

A. E. Blinov, V. E. Blinov, V. P. Druzhinin, V. B. Golubev, V. N. Ivanchenko, E. A. Kravchenko, A. P. Onuchin, S. I. Serednyakov, Yu. I. Skovpen, E. P. Solodov, A. N. Yushkov

Budker Institute of Nuclear Physics, Novosibirsk 630090, Russia

D. Best, M. Bruinsma, M. Chao, I. Eschrich, D. Kirkby, A. J. Lankford, M. Mandelkern, R. K. Mommsen, W. Roethel, D. P. Stoker

University of California at Irvine, Irvine, CA 92697, USA

C. Buchanan, B. L. Hartfiel

University of California at Los Angeles, Los Angeles, CA 90024, USA

S. D. Foulkes, J. W. Gary, B. C. Shen, K. Wang

University of California at Riverside, Riverside, CA 92521, USA

D. del Re, H. K. Hadavand, E. J. Hill, D. B. MacFarlane, H. P. Paar, Sh. Rahatlou, V. Sharma

University of California at San Diego, La Jolla, CA 92093, USA

J. W. Berryhill, C. Campagnari, B. Dahmes, O. Long, A. Lu, M. A. Mazur, J. D. Richman, W. Verkerke

University of California at Santa Barbara, Santa Barbara, CA 93106, USA

T. W. Beck, A. M. Eisner, C. A. Heusch, J. Kroseberg, W. S. Lockman, G. Nesom, T. Schalk, B. A. Schumm, A. Seiden, P. Spradlin, D. C. Williams, M. G. Wilson

University of California at Santa Cruz, Institute for Particle Physics, Santa Cruz, CA 95064, USA

J. Albert, E. Chen, G. P. Dubois-Felsmann, A. Dvoretskii, D. G. Hitlin, I. Narsky, T. Piatenko, F. C. Porter, A. Ryd, A. Samuel, S. Yang

California Institute of Technology, Pasadena, CA 91125, USA

S. Jayatilleke, G. Mancinelli, B. T. Meadows, M. D. Sokoloff

University of Cincinnati, Cincinnati, OH 45221, USA

T. Abe, F. Blanc, P. Bloom, S. Chen, W. T. Ford, U. Nauenberg, A. Olivas, P. Rankin, J. G. Smith, J. Zhang, L. Zhang

University of Colorado, Boulder, CO 80309, USA

A. Chen, J. L. Harton, A. Soffer, W. H. Toki, R. J. Wilson, Q. Zeng

Colorado State University, Fort Collins, CO 80523, USA

D. Altenburg, T. Brandt, J. Brose, M. Dickopp, E. Feltresi, A. Hauke, H. M. Lacker,
R. Müller-Pfefferkorn, R. Nogowski, S. Otto, A. Petzold, J. Schubert, K. R. Schubert,
R. Schwierz, B. Spaan, J. E. Sundermann

*Technische Universität Dresden, Institut für Kern- und Teilchenphysik, D-01062 Dresden,
Germany*

D. Bernard, G. R. Bonneaud, F. Brochard, P. Grenier, S. Schrenk, Ch. Thiebaux, G. Vasileiadis,
M. Verderi

Ecole Polytechnique, LLR, F-91128 Palaiseau, France

D. J. Bard, P. J. Clark, D. Lavin, F. Muheim, S. Playfer, Y. Xie

University of Edinburgh, Edinburgh EH9 3JZ, United Kingdom

M. Andreotti, V. Azzolini, D. Bettoni, C. Bozzi, R. Calabrese, G. Cibinetto, E. Luppi,
M. Negrini, L. Piemontese, A. Sarti

Università di Ferrara, Dipartimento di Fisica and INFN, I-44100 Ferrara, Italy

E. Treadwell

Florida A&M University, Tallahassee, FL 32307, USA

F. Anulli, R. Baldini-Ferroli, A. Calcaterra, R. de Sangro, G. Finocchiaro, P. Patteri,
I. M. Peruzzi, M. Piccolo, A. Zallo

Laboratori Nazionali di Frascati dell'INFN, I-00044 Frascati, Italy

A. Buzzo, R. Capra, R. Contri, G. Crosetti, M. Lo Vetere, M. Macri, M. R. Monge, S. Passaggio,
C. Patrignani, E. Robutti, A. Santroni, S. Tosi

Università di Genova, Dipartimento di Fisica and INFN, I-16146 Genova, Italy

S. Bailey, G. Brandenburg, K. S. Chaisanguanthum, M. Morii, E. Won

Harvard University, Cambridge, MA 02138, USA

R. S. Dubitzky, U. Langenegger

Universität Heidelberg, Physikalisches Institut, Philosophenweg 12, D-69120 Heidelberg, Germany

W. Bhimji, D. A. Bowerman, P. D. Dauncey, U. Egede, J. R. Gaillard, G. W. Morton, J. A. Nash,
M. B. Nikolich, G. P. Taylor

Imperial College London, London, SW7 2AZ, United Kingdom

M. J. Charles, G. J. Grenier, U. Mallik

University of Iowa, Iowa City, IA 52242, USA

J. Cochran, H. B. Crawley, J. Lamsa, W. T. Meyer, S. Prell, E. I. Rosenberg, A. E. Rubin, J. Yi

Iowa State University, Ames, IA 50011-3160, USA

M. Biasini, R. Covarelli, M. Pioppi

Università di Perugia, Dipartimento di Fisica and INFN, I-06100 Perugia, Italy

M. Davier, X. Giroux, G. Grosdidier, A. Höcker, S. Laplace, F. Le Diberder, V. Lepeltier,
A. M. Lutz, T. C. Petersen, S. Plaszczynski, M. H. Schune, L. Tantot, G. Wormser

Laboratoire de l'Accélérateur Linéaire, F-91898 Orsay, France

C. H. Cheng, D. J. Lange, M. C. Simani, D. M. Wright

Lawrence Livermore National Laboratory, Livermore, CA 94550, USA

A. J. Bevan, C. A. Chavez, J. P. Coleman, I. J. Forster, J. R. Fry, E. Gabathuler, R. Gamet,
D. E. Hutchcroft, R. J. Parry, D. J. Payne, R. J. Sloane, C. Touramanis

University of Liverpool, Liverpool L69 7ZE, United Kingdom

J. J. Back,[1] C. M. Cormack, P. F. Harrison,[1] F. Di Lodovico, G. B. Mohanty[1]

Queen Mary, University of London, E1 4NS, United Kingdom

C. L. Brown, G. Cowan, R. L. Flack, H. U. Flaecher, M. G. Green, P. S. Jackson,
T. R. McMahon, S. Ricciardi, F. Salvatore, M. A. Winter

*University of London, Royal Holloway and Bedford New College, Egham, Surrey TW20 0EX,
United Kingdom*

D. Brown, C. L. Davis

University of Louisville, Louisville, KY 40292, USA

---

[1]Now at Department of Physics, University of Warwick, Coventry, United Kingdom

J. Allison, N. R. Barlow, R. J. Barlow, P. A. Hart, M. C. Hodgkinson, G. D. Lafferty, A. J. Lyon,
J. C. Williams

University of Manchester, Manchester M13 9PL, United Kingdom

A. Farbin, W. D. Hulsbergen, A. Jawahery, D. Kovalskyi, C. K. Lae, V. Lillard, D. A. Roberts

University of Maryland, College Park, MD 20742, USA

G. Blaylock, C. Dallapiccola, K. T. Flood, S. S. Hertzbach, R. Kofler, V. B. Koptchev,
T. B. Moore, S. Saremi, H. Staengle, S. Willocq

University of Massachusetts, Amherst, MA 01003, USA

R. Cowan, G. Sciolla, S. J. Sekula, F. Taylor, R. K. Yamamoto

*Massachusetts Institute of Technology, Laboratory for Nuclear Science, Cambridge, MA 02139,
USA*

D. J. J. Mangeol, P. M. Patel, S. H. Robertson

McGill University, Montréal, QC, Canada H3A 2T8

A. Lazzaro, V. Lombardo, F. Palombo

Università di Milano, Dipartimento di Fisica and INFN, I-20133 Milano, Italy

J. M. Bauer, L. Cremaldi, V. Eschenburg, R. Godang, R. Kroeger, J. Reidy, D. A. Sanders,
D. J. Summers, H. W. Zhao

University of Mississippi, University, MS 38677, USA

S. Brunet, D. Côté, P. Taras

Université de Montréal, Laboratoire René J. A. Lévesque, Montréal, QC, Canada H3C 3J7

H. Nicholson

Mount Holyoke College, South Hadley, MA 01075, USA

N. Cavallo,[2] F. Fabozzi,[2] C. Gatto, L. Lista, D. Monorchio, P. Paolucci, D. Piccolo, C. Sciacca

*Università di Napoli Federico II, Dipartimento di Scienze Fisiche and INFN, I-80126, Napoli,
Italy*

---

[2]Also with Università della Basilicata, Potenza, Italy

M. Baak, H. Bulten, G. Raven, H. L. Snoek, L. Wilden

NIKHEF, National Institute for Nuclear Physics and High Energy Physics, NL-1009 DB Amsterdam, The Netherlands

C. P. Jessop, J. M. LoSecco

University of Notre Dame, Notre Dame, IN 46556, USA

T. Allmendinger, K. K. Gan, K. Honscheid, D. Hufnagel, H. Kagan, R. Kass, T. Pulliam, A. M. Rahimi, R. Ter-Antonyan, Q. K. Wong

Ohio State University, Columbus, OH 43210, USA

J. Brau, R. Frey, O. Igonkina, C. T. Potter, N. B. Sinev, D. Strom, E. Torrence

University of Oregon, Eugene, OR 97403, USA

F. Colecchia, A. Dorigo, F. Galeazzi, M. Margoni, M. Morandin, M. Posocco, M. Rotondo, F. Simonetto, R. Stroili, G. Tiozzo, C. Voci

Università di Padova, Dipartimento di Fisica and INFN, I-35131 Padova, Italy

M. Benayoun, H. Briand, J. Chauveau, P. David, Ch. de la Vaissière, L. Del Buono, O. Hamon, M. J. J. John, Ph. Leruste, J. Malcles, J. Ocariz, M. Pivk, L. Roos, S. T'Jampens, G. Therin

Universités Paris VI et VII, Laboratoire de Physique Nucléaire et de Hautes Energies, F-75252 Paris, France

P. F. Manfredi, V. Re

Università di Pavia, Dipartimento di Elettronica and INFN, I-27100 Pavia, Italy

P. K. Behera, L. Gladney, Q. H. Guo, J. Panetta

University of Pennsylvania, Philadelphia, PA 19104, USA

C. Angelini, G. Batignani, S. Bettarini, M. Bondioli, F. Bucci, G. Calderini, M. Carpinelli, F. Forti, M. A. Giorgi, A. Lusiani, G. Marchiori, F. Martinez-Vidal,[3] M. Morganti, N. Neri, E. Paoloni, M. Rama, G. Rizzo, F. Sandrelli, J. Walsh

Università di Pisa, Dipartimento di Fisica, Scuola Normale Superiore and INFN, I-56127 Pisa, Italy

M. Haire, D. Judd, K. Paick, D. E. Wagoner

Prairie View A&M University, Prairie View, TX 77446, USA

---

[3]Also with IFIC, Instituto de Física Corpuscular, CSIC-Universidad de Valencia, Valencia, Spain

N. Danielson, P. Elmer, Y. P. Lau, C. Lu, V. Miftakov, J. Olsen, A. J. S. Smith, A. V. Telnov

Princeton University, Princeton, NJ 08544, USA

F. Bellini, G. Cavoto,[4] R. Faccini, F. Ferrarotto, F. Ferroni, M. Gaspero, L. Li Gioi,
M. A. Mazzoni, S. Morganti, M. Pierini, G. Piredda, F. Safai Tehrani, C. Voena

Università di Roma La Sapienza, Dipartimento di Fisica and INFN, I-00185 Roma, Italy

S. Christ, G. Wagner, R. Waldi

Universität Rostock, D-18051 Rostock, Germany

T. Adye, N. De Groot, B. Franek, N. I. Geddes, G. P. Gopal, E. O. Olaiya

Rutherford Appleton Laboratory, Chilton, Didcot, Oxon, OX11 0QX, United Kingdom

R. Aleksan, S. Emery, A. Gaidot, S. F. Ganzhur, P.-F. Giraud, G. Hamel de Monchenault,
W. Kozanecki, M. Legendre, G. W. London, B. Mayer, G. Schott, G. Vasseur, Ch. Yèche, M. Zito

DSM/Dapnia, CEA/Saclay, F-91191 Gif-sur-Yvette, France

M. V. Purohit, A. W. Weidemann, J. R. Wilson, F. X. Yumiceva

University of South Carolina, Columbia, SC 29208, USA

D. Aston, R. Bartoldus, N. Berger, A. M. Boyarski, O. L. Buchmueller, R. Claus, M. R. Convery,
M. Cristinziani, G. De Nardo, D. Dong, J. Dorfan, D. Dujmic, W. Dunwoodie, E. E. Elsen, S. Fan,
R. C. Field, T. Glanzman, S. J. Gowdy, T. Hadig, V. Halyo, C. Hast, T. Hryn'ova, W. R. Innes,
M. H. Kelsey, P. Kim, M. L. Kocian, D. W. G. S. Leith, J. Libby, S. Luitz, V. Luth, H. L. Lynch,
H. Marsiske, R. Messner, D. R. Muller, C. P. O'Grady, V. E. Ozcan, A. Perazzo, M. Perl,
S. Petrak, B. N. Ratcliff, A. Roodman, A. A. Salnikov, R. H. Schindler, J. Schwiening, G. Simi,
A. Snyder, A. Soha, J. Stelzer, D. Su, M. K. Sullivan, J. Va'vra, S. R. Wagner, M. Weaver,
A. J. R. Weinstein, W. J. Wisniewski, M. Wittgen, D. H. Wright, A. K. Yarritu, C. C. Young

Stanford Linear Accelerator Center, Stanford, CA 94309, USA

P. R. Burchat, A. J. Edwards, T. I. Meyer, B. A. Petersen, C. Roat

Stanford University, Stanford, CA 94305-4060, USA

S. Ahmed, M. S. Alam, J. A. Ernst, M. A. Saeed, M. Saleem, F. R. Wappler

State University of New York, Albany, NY 12222, USA

---

[4]Also with Princeton University, Princeton, USA

W. Bugg, M. Krishnamurthy, S. M. Spanier

University of Tennessee, Knoxville, TN 37996, USA

R. Eckmann, H. Kim, J. L. Ritchie, A. Satpathy, R. F. Schwitters

University of Texas at Austin, Austin, TX 78712, USA

J. M. Izen, I. Kitayama, X. C. Lou, S. Ye

University of Texas at Dallas, Richardson, TX 75083, USA

F. Bianchi, M. Bona, F. Gallo, D. Gamba

Università di Torino, Dipartimento di Fisica Sperimentale and INFN, I-10125 Torino, Italy

L. Bosisio, C. Cartaro, F. Cossutti, G. Della Ricca, S. Dittongo, S. Grancagnolo, L. Lanceri,
P. Poropat,[5] L. Vitale, G. Vuagnin

Università di Trieste, Dipartimento di Fisica and INFN, I-34127 Trieste, Italy

R. S. Panvini

Vanderbilt University, Nashville, TN 37235, USA

Sw. Banerjee, C. M. Brown, D. Fortin, P. D. Jackson, R. Kowalewski, J. M. Roney, R. J. Sobie

University of Victoria, Victoria, BC, Canada V8W 3P6

H. R. Band, B. Cheng, S. Dasu, M. Datta, A. M. Eichenbaum, M. Graham, J. J. Hollar,
J. R. Johnson, P. E. Kutter, H. Li, R. Liu, A. Mihalyi, A. K. Mohapatra, Y. Pan, R. Prepost,
P. Tan, J. H. von Wimmersperg-Toeller, J. Wu, S. L. Wu, Z. Yu

University of Wisconsin, Madison, WI 53706, USA

M. G. Greene, H. Neal

Yale University, New Haven, CT 06511, USA

---

[5]Deceased

1 INTRODUCTION

The purpose of this analysis is the simultaneous measurement of the branching fraction, the longitudinal-polarization component, and the direct-CP-violating charge asymmetry for the $B \to$ vector-vector decay mode $B^+ \to K^{*0}\rho^+$, which has previously not been seen experimentally. The measurement of the polarization of this penguin decay is of special interest. There is no tree contribution to the decay amplitude and only a very small annihilation process. The polarization of the $B^+ \to K^{*0}\rho^+$ decay mode can be compared to that already measured for the similar penguin decay $B \to K^*\phi$. The direct-CP-violating charge asymmetry is defined as:

$$\mathcal{A}_{CP} \equiv \frac{N(B^- \to K^{*0}\rho^-) - N(B^+ \to \overline{K}^{*0}\rho^+)}{N(B^- \to K^{*0}\rho^-) + N(B^+ \to \overline{K}^{*0}\rho^+)}.$$

In this penguin decay, a value significantly different from zero could be a hint for new physics.

1.1 Physics motivation

In the Standard Model, the study of the penguin decay $B^+ \to K^{*0}\rho^+$, combined with information from other charmless hadronic $B \to$ vector-vector decays into $K^*\rho$ and $\rho\rho$, allows us to constrain the angles α and γ of the unitarity triangle, in a way similar to the study of the $B \to \pi\pi$ and $B \to K\pi$ decays [1]. The $\rho\rho$ modes are used to constrain the angle α. The methods that constrain the angle γ are based on isospin symmetry relationships relating the amplitudes of the different $K^*\rho$ decay modes, as well as on the $SU(3)$ flavour symmetry relating the $K^*\rho$ and $\rho\rho$ modes. They also rely on the relationship $\alpha = \pi - \beta - \gamma$ and the measured value of the angle β. A constraint on γ can already be obtained using only the charged-B decays $B^+ \to K^{*0}\rho^+$, $B^+ \to K^{*+}\rho^0$, and $B^+ \to \rho^+\rho^0$ [2]. The two modes $B^+ \to K^{*+}\rho^0$ and $B^+ \to \rho^+\rho^0$ have been studied previously [3, 4]. A stronger constraint on γ can be obtained by including the $B^0 \to K^{*+}\rho^-$ mode, a first study of which is also being presented at this conference and is based on a similar analysis technique [5].

Measurements of the rates, polarizations, and direct-CP-violating asymmetries of these vector-vector decays permit testing theoretical predictions from the naive factorization [6] and QCD factorization [7, 8] based models.

In charmless decays of B mesons into two light vector mesons, both longitudinal and transverse polarization states are possible, but a large longitudinal-polarization fraction, of order $1 - 4 \times \frac{m_\rho^2}{m_B^2} \approx 0.9$ for $K^*\rho$, is expected from theory for both tree and penguin decays. Existing measurements of tree dominated vector-vector charmless modes $\rho^+\rho^-$ and $\rho^+\rho^0$ show that their longitudinal component is indeed dominant [3, 4, 9]. However, experimental results for the polarization in the pure gluonic penguin $B^0 \to \phi K^{*0}$ and $B^+ \to \phi K^{*+}$ charmless processes indicate a transverse polarization fraction of about 0.5 [10, 11, 3]. This difference can be accounted for in the Standard Model by increasing the non-factorizable contribution of annihilation diagrams, through the tuning of some poorly known non-perturbative QCD parameters [8, 12, 13]. The uncertainty on these parameters makes the accurate *a priori* prediction of the polarization difficult for a given decay mode. However, using SU(3) flavour

symmetry arguments, the same polarization is expected for the $B^+ \to K^{*0}\rho^+$ decay and for $B \to \phi K^*$ decays.

Thus, the comparison of the polarizations obtained in the two penguin modes $B^+ \to K^{*0}\rho^+$ and ϕK^* is of interest since the ~ 0.5 transverse polarization fraction observed in ϕK^* decays could also be due to contributions from new physics in the penguin loop.

Table 1 summarizes the theoretical predictions from the naive-factorization model compared to the existing measurements of branching fractions and polarizations for the $K^*\rho$ and $\rho\rho$ decay modes. The theoretical predictions for the branching fractions are taken from [6]. They have been updated in [14]. The ranges given are obtained by varying the form factors and other parameters entering the calculation. The polarizations have also been predicted.

Table 1: Comparison of the predictions from the naive-factorization model to the measurements for the branching fractions and polarizations in the $K^*\rho$ and $\rho\rho$ decay modes. The branching fractions are in units of 10^{-6}. The results for $B^+ \to K^{*0}\rho^+$ are those reported here.

Mode	$\mathcal{B}$ (10^{-6}) prediction [6]	$\mathcal{B}$ (10^{-6}) prediction [14]	$\mathcal{B}$ (10^{-6}) Measurement	Polarization prediction [14]	Polarization measurement
$K^{*+}\rho^0$	6.6	$6-10$	$10.6^{+3.8}_{-3.5}$	0.90	$0.96^{+0.04}_{-0.16}$
$K^{*+}\rho^-$	7.0	$6-10$	< 17.2 @ 90% CL	0.90	$-$
$K^{*0}\rho^+$	9.0	$8-12$	$17.0^{+3.5}_{-3.9}$	0.90	0.79 ± 0.09
$\rho^+\rho^0$	6.1	$7-12$	$26.4^{+6.1}_{-6.4}$	0.92	0.89 ± 0.07
$\rho^+\rho^-$	24.0	$20-25$	27 ± 9	0.92	$0.98^{+0.02}_{-0.09}$

1.2 Angular analysis

The analysis is done in the helicity frame (Fig. 1) as a function of the "helicity angles" $\theta_{K^{*0}}$ and θ_{ρ^+}. The angle $\theta_{K^{*0}}$ (θ_{ρ^+}) is defined as the angle between the direction of the K^{*0} (ρ^+) and the direction of the π^- (π^0) coming from its decay in the vector meson's rest frame. An integration is performed over the angle ϕ between the vector-meson decay planes to simplify our analysis; this step is straightforward because the detector acceptance is independent of this angle. The longitudinal-polarization fraction f_L can be extracted from the differential decay rate, parametrized as a function of $\theta_{K^{*0}}$ and θ_{ρ^+} [15]:

$$\frac{1}{\Gamma}\frac{d^2\Gamma}{d\cos\theta_{K^{*0}}d\cos\theta_{\rho^+}} \propto \frac{1}{4}(1-f_L)\sin^2\theta_{K^{*0}}\sin^2\theta_{\rho^+} + f_L\cos^2\theta_{K^{*0}}\cos^2\theta_{\rho^+}. \qquad (1)$$

Experimentally, it is important to measure the branching fraction and the polarization simultaneously because of their large correlation. The two decay products of the vector mesons have in general comparable momenta when transversely polarized, and asymmetric momenta,
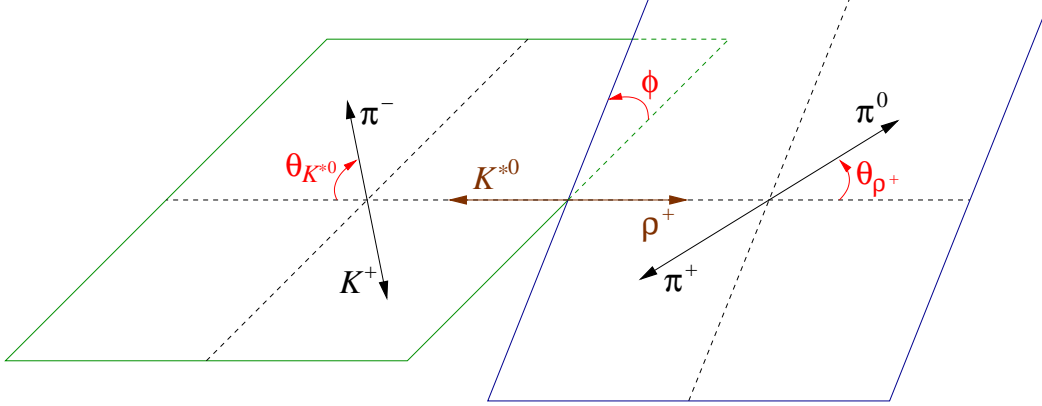
11

Figure 1: Helicity frames for the vector-vector $B^+ \to K^{*0}\rho^+$ decay.

with one high- and one low-momentum decay product, when longitudinally polarized. As soft particles have lower reconstruction efficiency, the efficiency for reconstructing longitudinally polarized decays is about half that for transversely polarized decays.

2 THE BABAR DETECTOR AND DATASET

The results presented in this paper are based on data collected in 1999-2002 with the BABAR detector [16] at the PEP-II asymmetric e^+e^- collider of the Stanford Linear Accelerator Center. An integrated luminosity of 81.85 fb^{-1} was recorded at the $\Upsilon(4S)$ resonance, corresponding to 88.84 ± 0.98 million $B\bar{B}$ pairs. An additional 9.58 fb^{-1} data sample taken 40 MeV below the $\Upsilon(4S)$ resonance is used in order to study the continuum background $e^+e^- \to q\bar{q}$ ($q = u, d, s, c$).

Charged particles are detected and their momenta measured with the combination of a silicon vertex tracker with five layers of double-sided detectors and a 40-layer central drift chamber, both operating in the 1.5-T magnetic field of a solenoid. Charged-particle identification (PID) is provided by measurement of the average energy loss (dE/dx) in the tracking devices and by an internally reflecting ring-imaging Cherenkov detector covering the central region. A K/π separation of better than four standard deviations (σ) is achieved for momenta below 3 GeV/c, decreasing to 2.5 σ at the highest momenta found in B decay. Photons and electrons are detected by a CsI(Tl) electromagnetic calorimeter (EMC).

3 ANALYSIS METHOD

We reconstruct $B^+ \to K^{*0}\rho^+$ candidates through the decays $K^{*0} \to K^+\pi^-$ and $\rho^+ \to \pi^+\pi^0$, $\pi^0 \to \gamma\gamma$. Inclusion of the charge conjugate processes is implied in this paper.

The main backgrounds are from continuum events and $B\bar{B}$ events (B background). Event

selection reduces these backgrounds but as a maximum likelihood fit will be performed the selection is kept loose. Some non-resonant charmless B decays into four bodies are a particular problem as they have similar final states to our signal and their branching fractions are poorly known.

3.1 Selection and discriminating variables

Monte Carlo (MC) simulations [17] of the signal and the B background as well as the off-resonance beam data were used to determine the selection criteria before the examination of the on-resonance beam data.

The final state of the signal decay is $K^+\pi^+\pi^-\pi^0$. We first select charged kaons and pions from charged tracks. Charged tracks candidates are required to originate from the interaction point: distance of closest approach to the interaction point less than 10 cm along the beam directions, and less than 1.5 cm in the plane transverse to the beam directions. We require that the charged pion candidates from the K^{*0} and ρ^+ decays not be identified as electrons, kaons, or protons, and that the charged kaon candidate from the K^{*0} decay agrees with a kaon hypothesis and be inconsistent with the electron and proton hypotheses.

Next, we reconstruct π^0 candidates from photon pairs, where each photon has an energy larger than 50 MeV and exhibits a lateral profile of energy deposition in the EMC consistent with an electromagnetic shower [16]. The π^0 candidate mass must satisfy $0.11 < m_{\gamma\gamma} < 0.16$ GeV/c^2.

We then reconstruct K^{*0} and ρ^+ candidates. The mass of the $K^{\star 0}$ and the ρ^+ candidates must satisfy $|m_{K^+\pi^-} - 0.896| < 0.125$ GeV/c^2 and $|m_{\pi^+\pi^0} - 0.769| < 0.375$ GeV/c^2. These mass windows correspond to about 2.5 times the resonance full width (Fig. 3). Combinatorial backgrounds dominate near the helicity angle regions $|\cos\theta_{K^{*0},\rho^+}| = 1$, where the vector mesons tend to decay in a way that produces a soft particle. The effect is more important when this soft particle is a π^0. If one assumes that the longitudinal polarization is large, as suggested by recent measurements of charmless vector-vector modes and theoretical predictions, it is important to maintain the largest possible coverage in $\cos\theta_{K^{*0},\rho^+}$. The requirements $-0.95 < \cos\theta_{K^{*0}} < 1.0$ ($-0.8 < \cos\theta_{\rho^+} < 0.95$) are applied to reject candidates with a soft π^- (π^0 and π^+) coming from the K^{*0} (ρ^+) decay; they allow the suppression of most of the combinatorial backgrounds while maintaining adequate efficiency for longitudinally-polarized decays.

We select B candidates from the $K^{*0}\rho^+$ combinations using two nearly independent kinematic observables [16], the beam energy-substituted B mass $m_{ES} \equiv \sqrt{(\frac{s}{2} + \mathbf{p}_i \mathbf{p}_B)^2/E_i^2 - p_B^2}$ and the energy difference $\Delta E \equiv (E_i E_B - \mathbf{p}_i \cdot \mathbf{p}_B - \frac{s}{2})/\sqrt{s}$, where $\sqrt{s}$ is the beam energy in the $\Upsilon(4S)$ CM, and $(E_B, \mathbf{p}_B)$ and $(E_i, \mathbf{p}_i)$ are the four-momenta of the B candidate and the e^+e^- initial state, both defined in the laboratory frame. For signal events, the m_{ES} distribution peaks at the B-meson mass and the ΔE distribution peaks near zero. We require B candidates to satisfy $5.21 < m_{ES} < 5.29$ GeV/c^2 and $|\Delta E| < 0.15$ GeV. When multiple B candidates exist in the same event, we select the one whose reconstructed π^0

mass is nearest to the known π^0 mass; we choose the candidate randomly from those that share the same π^0.

To discriminate signal from continuum background, we also use a neural network (NN) combining six variables: a Fisher discriminant made from two event-shape variables (see [18]); the cosine of the angle between the direction of the B and the collision axis (z) in the CM frame; the cosine of the angle between the B-thrust axis and the z axis; the cosine of the angle between the B-thrust axis and the thrust of the particles of the rest of the event; the angle between the direction of the π^0 and that of one of its daughter photons in the π^0 rest frame (π^0 decay angle); and the sum of transverse momenta relative to the z-axis of the particles in the rest of the event.

3.2 Sample composition

The expected numbers of signal and background events in the data sample are summarized in Table 2. The B background is divided into categories, described below, that are modeled separately in the maximum likelihood fit (Sec. 3.3).

Table 2: Number of events expected in the $K^{*0}\rho^+$ analysis for an 81.85 fb^{-1} data sample. A branching fraction of 20×10^{-6} and a longitudinal polarization of 75% are assumed for the signal.

Category	Expected number of events
Signal	167
Continuum	12400
$b \to charm$ backgrounds	
$B^+ \to \bar{D}^0 \pi^+$	409
$B^+ \to \bar{D}^0 \rho^+$	696
$B^+ \to c$, excluding $\bar{D}^0 \pi^+$ and $\bar{D}^0 \rho^+$	915
$B^0 \to c$	904
$b \to charmless$ backgrounds	
$\rho^+ \rho^0$ (100% longitudinal polarization)	3.2
$K^{*0} \pi^0$	4.3
"Five bodies"	68
"Other Charmless"	291

3.2.1 Signal

The signal consists of correctly reconstructed "true signal" events as well as badly recon-structed "Self-Cross-Feed" (SxF) events. SxF events contain useful information as one of

the two vector mesons is usually correctly reconstructed. They are treated separately in the fit.

The SxF events are due mostly to the misassignment of a charged (neutral) pion in about 60% (40%) of the cases. The SxF events are decomposed into three categories: events in which the K^{*0} is reconstructed correctly but not the ρ^+, events in which the ρ^+ is reconstructed correctly but not the K^{*0}, and events in which neither vector meson is reconstructed correctly.

The total signal selection efficiency, including both "true signal" and SxF events, is $12.6 \pm 0.1\%$ ($20.6 \pm 0.2\%$) for longitudinally (transversely) polarized events. The fraction of SxF events is $25.1 \pm 0.2\%$ ($10.9 \pm 0.3\%$) for longitudinally (transversely) polarized events.

3.2.2 B background

Background from B decays can be split into that from $b \rightarrow c$ transitions and that from $b \rightarrow charmless$ transitions. We further split the $b \rightarrow c$ background into four subcategories, each with its own term in the likelihood fit (Sec. 3.3): $B^+ \rightarrow \bar{D}^0 \pi^+$, $B^+ \rightarrow \bar{D}^0 \rho^+$, $B^+ \rightarrow charm$ other than the first two, and $B^0 \rightarrow charm$. The first two peak in m_{ES} while the last two do not. In particular, $B^+ \rightarrow \bar{D}^0 \pi^+$, $\bar{D}^0 \rightarrow K^+ \pi^- \pi^0$ and $B^+ \rightarrow \bar{D}^0 \rho^+$, $\bar{D}^0 \rightarrow K^+ \pi^-$ share the same final state $K^+ \pi^+ \pi^- \pi^0$ with signal.

The other charmless B backgrounds are modeled in four categories in the likelihood fit. The two $B^+ \rightarrow \rho^+ \rho^0$ and $B^0 \rightarrow K^{*0} \pi^0$ specific modes are separated due to their similarity with the signal. The rest of the charmless are divided into two additional categories. The "five bodies" category includes decay modes that have five particles in the final state and involve an intermediate resonance $[a_1^0, a_1^+, a_0^0, a_0^+, \omega, f_0, \rho^+, \rho^0, K^{*+}, K^{*0}]$ or one of the particles K^+, π^+ or π^0. The "Other Charmless" category consists of all other charmless modes after all the above modes have been excluded. The modes in the "five bodies" category resemble the signal more than the ones in the "Other Charmless" category due to the resonances. Therefore their m_{ES} distribution peaks slightly more at the B-meson mass. However the yield of the "Other Charmless" category is four times larger (Table 2). Since it is the most poorly known, it will be floated in the likelihood fit.

None of the non-resonant charmless modes $K^{*0} \pi^+ \pi^0$, $K^+ \rho^+ \pi^-$, and $K^+ \pi^+ \pi^- \pi^0$, with the same final state as the signal, have been studied experimentally. No theoretical model is currently available to predict their branching ratios and their decay kinematics. Therefore they are not modeled in the likelihood fit in this preliminary analysis. Yet they could produce substantial false signals since their final state is the same as for signal events. A systematic error will be assigned for this fact (Sec. 4.4).

To summarize, we have a total of 13 categories of events: the "true signal", three SxF categories, the continuum, four categories of charm B-background, and four categories of charmless B-background. In the fit, we float the sum of the yields in the "true signal" and the SxF categories, as well as the yields in the continuum and the "Other Charmless" categories. The yields in all the other B-background categories are fixed.

3.3 Likelihood fit

We perform an unbinned, extended maximum likelihood fit on the selected data sample to extract the signal yield, the longitudinal polarization f_L, and the direct-CP-violating asymmetry $\mathcal{A}_{CP}$. Seven observables are used: m_{ES}, ΔE, the helicity angles $\cos(\theta_{K^{*0}})$ and $\cos(\theta_{\rho^+})$, the reconstructed masses of the two vectors $m_{K^{*0}}$ and m_{ρ^+}, and the neural network output.

All significant correlations are taken into account in the likelihood function described below or are covered by systematic errors (Sec. 4.2.1).

The extended likelihood function is then given by:

$$
L = e^{-N'} \prod_{i=1}^{N} \left(n_{sig}(f_{Sig}^{true} P_{Sig,i} + \sum_{SxF_k=1,3} f_{SxF_k} P_{SxF_k,i}) + n_{cont} P_{cont,i} + \sum_{\substack{B \ backg. \\ j}} n_j P_{j,i} \right) \quad (2)
$$

where n_{sig} and n_{cont} are the numbers of signal (including SxF) and continuum events that are floated in the fit. The numbers of events n_j in the B-background category j are all fixed to their Monte-Carlo expectations, except in the case of the "Other Charmless" category for which the yield is floated. $N'(N)$ are the expected (observed) total numbers of events in the data sample and i is the event index. f_{Sig}^{true} and $f_{SxF_{1,3}}$ are the fractions of "true signal" and of the three different SxF categories normalized to the total number of signal events n_{sig}. These fractions are different in the longitudinal and transverse components and are taken from the simulation.

The normalized P Probability Density Function (PDF) in each category is the product of the normalized PDFs of each observable, except for the continuum for which a joint PDF of the correlated helicities and vector-meson masses is used.

PDF Models

The m_{ES}, ΔE, NN, $\cos\theta_{K^{*0}}$, $\cos\theta_{\rho^+}$, $m_{K^{*0}}$, and m_{ρ^+} PDFs of the "true signal" and the B background are taken from the simulation, but the means and widths of the signal Gaussian PDFs for m_{ES} and ΔE are corrected to account for the differences between data and Monte-Carlo observed in a $B^+ \to \bar{D}^0 \pi^+$ (with $\bar{D}^0 \to K^+ \pi^- \pi^0$) control samples.

For the signal including the three SxF categories, the distributions of the vector masses and helicities are modeled using for each vector meson the distributions of equation (1) modified by a function $a_{K^{*0},\rho^+}(\theta_{K^{*0},\rho^+})$ proportional to the probability for a signal event to be reconstructed, correctly or not, and multiplied by the probability $P_{K^{*0},\rho^+}^{true}(\theta_{K^{*0},\rho^+})$ $(1 - P_{K^{*0},\rho^+}^{true}(\theta_{K^{*0},\rho^+}))$ to reconstruct correctly (or not) the K^{*0} or the ρ^+; both functions depend on the vector-meson helicity angle. Different mass distributions $Pm_{K^{*0},\rho^+}^{True,False}(m_{K^{*0},\rho^+})$ of the vector-meson mass m_{K^{*0},ρ^+} are used whether the reconstruction of the meson is correct or not. For example, for the "true signal" longitudinal component we have: $a_{K^{*0}}(\theta_{K^{*0}})a_{\rho^+}(\theta_{\rho^+})$ $\times P_{K^{*0}}^{true}(\theta_{K^{*0}})P_{\rho^+}^{true}(\theta_{\rho^+}) \times \cos^2(\theta_{K^{*0}})\cos^2(\theta_{\rho^+}) \times Pm_{K^{*0}}^{True}(m_{K^{*0}})Pm_{\rho^+}^{True}(m_{\rho^+})$. Another example is the transverse component of the SxF category with a correctly reconstructed K^{*0} described by: $a_{K^{*0}}(\theta_{K^{*0}})a_{\rho^+}(\theta_{\rho^+}) \times P_{K^{*0}}^{true}(\theta_{K^{*0}})(1 - P_{\rho^+}^{true}(\theta_{\rho^+})) \times \sin^2(\theta_{K^{*0}})\sin^2(\theta_{\rho^+}) \times$

16

Table 3: Summary of the multiplicative systematic uncertainties ΔB on the branching fraction $\mathcal{B}$ associated with the signal reconstruction efficiency and number of $B\overline{B}$.

Source	ΔB
π^0reconstruction	8.6 %
Track reconstruction	3.9 %
PID	1.1 %
Number of $B\overline{B}$ pairs	1.1 %
Total	9.6 %

$Pm_{K^{*0}}^{True}(m_{K^{*0}})Pm_{\rho^+}^{False}(m_{\rho^+})$. The model supposes that the reconstruction of the two vector mesons is independent. A systematic uncertainty for this assumption is included in the total uncertainty (Sec. 4.2.1).

In the continuum, the m_{ES} distribution is parametrized by an ARGUS function [19], the ΔE distribution by a second order polynomial, and the neural network output (NN) distribution by the three-parameter function $(1 - NN)^{(a_1 + a_2(1-NN) + a_3(1-NN)^2)}$. The shape parameters entering the PDFs of the m_{ES}, ΔE, and NN observables are also floated in the fit: the statistics of the "on-resonance" data is much larger than the "off-resonance" data, which is used for cross-checks. To model the correlation between the mass and the helicity of each vector meson, non-parametric PDFs are made from two 2-dimensional mass-helicity histograms extracted from the m_{ES} side-band ($m_{ES} < 5.25$ GeV/c^2 and $NN < 0.4$), after subtraction of the remaining B background (less than 10%).

4   SYSTEMATIC UNCERTAINTIES

The systematic uncertainties are summarized in Tables 3 and 4. Table 3 displays the uncertainties on the efficiency of signal reconstruction and on the total number of $B\bar{B}$ pairs in the data set, each which contributes to a multiplicative uncertainty on the final branching fraction. The quadratic sum of the uncertainties in Table 3 is reported in Table 4 as "Signal reconstruction efficiency, number of $B\overline{B}$ pairs." It is one of the largest contributions to the overall systematic uncertainty on the branching fraction measurement.

4.1   Fractions of "True signal" and SxF categories, and efficiencies

Table 4 also gives the systematic uncertainties on the polarization f_L, due to the uncertainty on the ratio of the selection efficiencies for the longitudinal and transverse polarization components (used to compute the effective polarization of the selected signal events).

Other systematics on the signal yield and the polarization are due to the uncertainties on the relative fractions f_{Sig}^{true} and $f_{SxF_{1,2,3}}$ of the "pure signal" and of the three SxF categories,

Table 4: Summary of the systematic uncertainties on the signal yield, on the branching fraction, and on the polarization. The asymmetric uncertainty from the non-resonant charmless backgrounds is presented separately from the other systematics.

Source	N_S	$\mathcal{B}$	f_L
Signal reconstruction efficiency, number of $B\bar{B}$ pairs	$-$	9.6%	$-$
Ratio of efficiencies for long./trans. polarizations	±0.0	$\pm0.0\%$	±0.006
"True signal" and Self-cross-feed fractions	±1.7	$\pm1.2\%$	±0.001
PDF shapes	±6.4	$\pm4.5\%$	±0.019
NN shape in off-resonance data	±4.9	$\pm3.5\%$	±0.027
No. B backgrounds	±1.8	$\pm1.3\%$	±0.010
Total	±8.4	$\pm11.3\%$	±0.035
Non-resonant charmless backgrounds ($K^+\pi^+\pi^-\pi^0$ final state)	-15.7	-11.1%	±0.020

which are taken from the simulation. Due to correlations between the K^* and ρ detection and reconstruction, the fraction of events in one category of signal or SxF is slightly different from the product of the probabilities $P^{true}_{K^{*0},\ \rho^+}(\theta_{K^{*0},\ \rho^+})$ (Sec. 3.3) to reconstruct correctly or not the vector meson, averaged over the helicity angles. The difference between the results obtained with this set of signal and SxF fractions and the set of values taken directly from the simulation is taken as the systematic uncertainty.

4.2 Uncertainties on PDFs shapes

The systematic labeled "PDF shapes" in Table 4 is due to the uncertainty of the PDF shapes for the signal, continuum, and B backgrounds. It includes the error on the correction of the mean and width of the "true signal" m_{ES} and ΔE gaussian distributions for the differences observed between the data and the simulation (Sec. 3.3). It includes also systematics associated with corrections of biases from the PDF models for the signal, SxF, and continuum (Sec. 4.2.1), and uncertainties due to the limited statistics in determining PDF shapes (Sec. 4.2.2).

4.2.1 Systematics from the PDF model itself

We first checked that the cut $\cos\theta_{\rho^+} > -0.8$ is sufficiently tight not to leave low momentum π^0 backgrounds that are not properly simulated: the results are stable when the analysis is repeated after a tighter selection on the helicity angle ($\cos\theta_{\rho^+} > -0.5$).

The model for the "true signal" and the SxF is tested using fully simulated signal, divided into sub-samples embedded in toy simulations of the other backgrounds. Each sample has the same number of signal events and the same polarization as is fitted in data. A small

bias of 4.1 ± 1.4 events is observed on the signal yield as well as a $(-1.2 \pm 0.5)\%$ bias on the polarization.

In the continuum, the masses and helicity distributions are modeled by using 2-dimensional mass-helicity histograms extracted from the m_{ES} side-band (Sec. 3.3). A slight bias of -2.2 ± 0.2 events on the signal yield and of $(-0.9 \pm 0.1)\%$ on the polarization is associated with this model. This is estimated using toy Monte-Carlo samples, generated with the PDF used for the data fit. For each toy experiment new PDFs of the masses and helicities of the vector mesons are constructed following the same procedure as in the real data sample. The results obtained when using the new PDFs are slightly biased compared to the results obtained when using the PDFs the toy sample was generated from.

The two biases from the signal and continuum models are corrected for in the final result, and conservative systematic errors, each equal to half of the correction, are assigned.

4.2.2 Systematics from the limited statistics to determine the PDFs

The systematic uncertainty associated to the shape of the parametrized PDFs is determined by varying the parameters within their statistical error obtained from a fit on the full simulation. The non-parametric PDFs are varied by generating toy samples using the original PDFs used in the real data fit. For each toy sample, new PDFs are made out of the generated distributions of the observables. The systematic error is the dispersion of the differences in the fit results between the new and the original PDFs.

4.2.3 Neural network shape parameters in the continuum

For the continuum, the m_{ES}, ΔE, and NN PDFs are parametrized. The parameters are determined from real data (Sec. 3.3). Their values agree with the values fitted on the off-resonance data for the m_{ES} and ΔE distributions, but not for the NN. A systematic uncertainty is assigned, labeled "NN shape in off-resonance data" in Table 4. It is equal to the difference on the results when using the two sets of parameters. Though it is an uncertainty on a PDF shape, it is displayed separately from the "PDF shapes" category as it is relatively large.

4.3 Number of events in the B-background categories

Other systematic uncertainties, labeled "No. B backgrounds" in Table 4, come from the uncertainty on the numbers of events in each B-background category that are fixed in the fit. The branching ratio of the $B^+ \to \rho^+ \rho^0$ decay is varied within the errors of the combined measurements of [3] and [4]: $\mathcal{B}(B^+ \to \rho^+ \rho^0) = (26.4^{+6.1}_{-6.4}) \times 10^{-6}$. The unknown branching fraction of the $K^{*0}\pi^0$ background mode is varied by 100%, assuming a central value of 7.5×10^{-6}. This value is half of the value of the measured branching fraction for the $K^{*0}\pi^+$ decay mode [20] ($\approx 15 \times 10^{-6}$), based on the isospin rule and the assumption of penguin

dominance. The number of events is varied by 20% in all the $b \to c$ categories and by 50% in the "Five bodies" category of charmless-B background. Note that there is no systematic error assigned for the "Other Charmless" category of events as this yield is floated in the fit to data.

4.4 Contribution from non-resonant charmless backgrounds decaying into $K^+\pi^+\pi^-\pi^0$

The non-resonant charmless B-decay modes $K^{*0}\pi^+\pi^0$, $K^+\rho^+\pi^-$, and $K^+\pi^+\pi^-\pi^0$ have the same final state as the signal and are not modeled in the fit. The associated systematic error is estimated by the difference in the data fit result when the yields of these background modes are floated or fixed to zero: PDFs of these modes can be constructed from their full simulation, based on a simplified phase space model, but the available statistics is limited to a few hundreds of events. We obtain an asymmetric error of -15.7 events (-11.1%) on the signal yield, which is systematically overestimated when these background modes are not modeled in the fit. We get an additional symmetric systematic error of 2.0% on the polarization. This main systematic error is a preliminary estimation and is presented separately from the other systematics, with the label "non-resonant".

Note that this study seems to show that most of these backgrounds are negligible, probably because their decay products populate different regions of the phase space. The only channel which has overlapping phase space is $(K^+\pi^-)_{S-wave}\rho^+$. A more detailed study of these backgrounds will be necessary.

5 PHYSICS RESULTS

We obtain from the fit $147.3^{+23.4}_{-22.3}$(stat) signal events and a longitudinal polarization fraction $f_L = 0.77 \pm 0.08$(stat). We then correct for the two small biases described in Section 4.2.1, from the models of the signal and self-cross-feed, and of the continuum. We obtain $141.0^{+23.4}_{-22.3}$(stat) ± 15.9(syst)$^{+0.0}_{-15.7}$(non-resonant) signal events and $f_L = 0.79 \pm 0.08$(stat) ± 0.04(syst) ± 0.02(non-resonant). The polarization observed is consistent with both the polarization found in the other pure penguin modes such as $K^*\phi$ $(f_L \sim 0.5)$ and with purely longitudinal polarization $(f_L \sim 1)$. From the number of signal events, the fraction of longitudinal polarization, the selection efficiencies determined for the transverse and longitudinal polarization components, and the branching fractions $\mathcal{B}(K^{*0} \to K^+\pi^-)$, $\mathcal{B}(\pi^0 \to \gamma\gamma)$, we compute the branching fraction:

$$\mathcal{B}(B^+ \to K^{*0}\rho^+) = [17.0 \pm 2.9(\text{stat}) \pm 2.0(\text{syst})^{+0.0}_{-1.9}(\text{non-resonant})] \times 10^{-6}.$$

The impact of the uncertainties on $\mathcal{B}(K^{*0} \to K^+\pi^-)$ and $\mathcal{B}(\pi^0 \to \gamma\gamma)$ is negligible compared to the other systematic errors. The statistical error on the branching fraction results from the statistical errors on the signal yield and the polarization, taking into account their correlation (Fig. 2). The systematic uncertainty on the branching fraction results from the
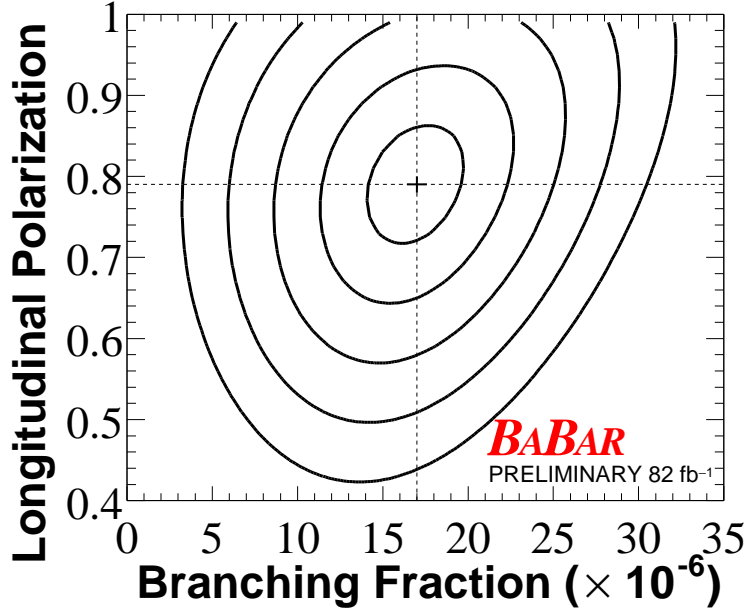
Figure 2: Countours at the 1, 2, 3, 4, and 5 σ levels showing the correlated statistical uncertainty on the branching fraction and on the polarization.

propagation of the systematics uncertainties on the signal yield and on the polarization. The systematic error on the signal yield (resp. polarization) of 15.9 events (resp. 4%), results in an systematic error of 1.9×10^{-6} (resp. 0.4×10^{-6}) on the branching fraction. Finally, the "non-resonant" systematics on the signal yield is propagated to the branching fraction.

This result is consistent with the isospin rule predicting that $\mathcal{B}(B^+ \to K^{*0}\rho^+) \approx 2\times \mathcal{B}(B^+ \to K^{*+}\rho^0)$, assuming the dominance of gluonic penguin diagrams in the $B^+ \to K^{*+}\rho^0$ decay and the measured $B^+ \to K^{*+}\rho^0$ branching fraction of $[10.6^{+3.8}_{-3.5}] \times 10^{-6}$ [3]. This result is about 2 standard deviations away from the predictions from naive factorization models [6, 14] (Table 1).

We also extract the direct-CP-violating charge asymmetry:

$$\mathcal{A}_{CP}(B^+ \to K^{*0}\rho^+) = [-14 \pm 17(\text{stat}) \pm 4(\text{syst})]\%.$$

It is consistent with zero, as expected for this pure penguin mode. The systematic uncertainties on $\mathcal{A}_{CP}$ arises from a limit on the possible size of charge-dependent tracking efficiency and particle identification biases. The uncertainty from the tracking is the linear sum of the 0.3% uncertainty for each charged track. The uncertainty from the particle identification is estimated at 4%.

The distributions of m_{ES}, ΔE, and the vector-meson helicities and reconstructed masses are shown in Figure 3 with the signal enriched by selecting events with large signal to background likelihood ratios on the discriminating variables not shown in each plot.

6 SUMMARY

We measure the branching fraction and the fraction of longitudinal component for the decay $B^+ \rightarrow K^{*0}\rho^+$ using a maximum likelihood technique. We use a data set corresponding to a total integrated luminosity of $81.85\,\text{fb}^{-1}$ taken on the $\Upsilon(4S)$ peak. A signal is observed for the first time with a significance of greater than 5σ. From a fitted signal yield of $141.0^{+23.4}_{-22.3}(\text{stat}) \pm 8.4(\text{syst})^{+0.0}_{-15.7}(\text{non-resonant})$ events we obtain the branching fraction:

$$\mathcal{B}(B^+ \rightarrow K^{*0}\rho^+) = [17.0 \pm 2.9(\text{stat}) \pm 2.0(\text{syst})^{+0.0}_{-1.9}(\text{non-resonant})] \times 10^{-6},$$

the longitudinal polarization fraction f_L:

$$f_L = 0.79 \pm 0.08(\text{stat}) \pm 0.04(\text{syst}) \pm 0.02(\text{non-resonant}),$$

and the direct-CP-violating asymmetry:

$$\mathcal{A}_{CP}(B^+ \rightarrow K^{*0}\rho^+) = [-14 \pm 17(\text{stat}) \pm 4(\text{syst})]\%.$$

These results are preliminary.

7 ACKNOWLEDGMENTS
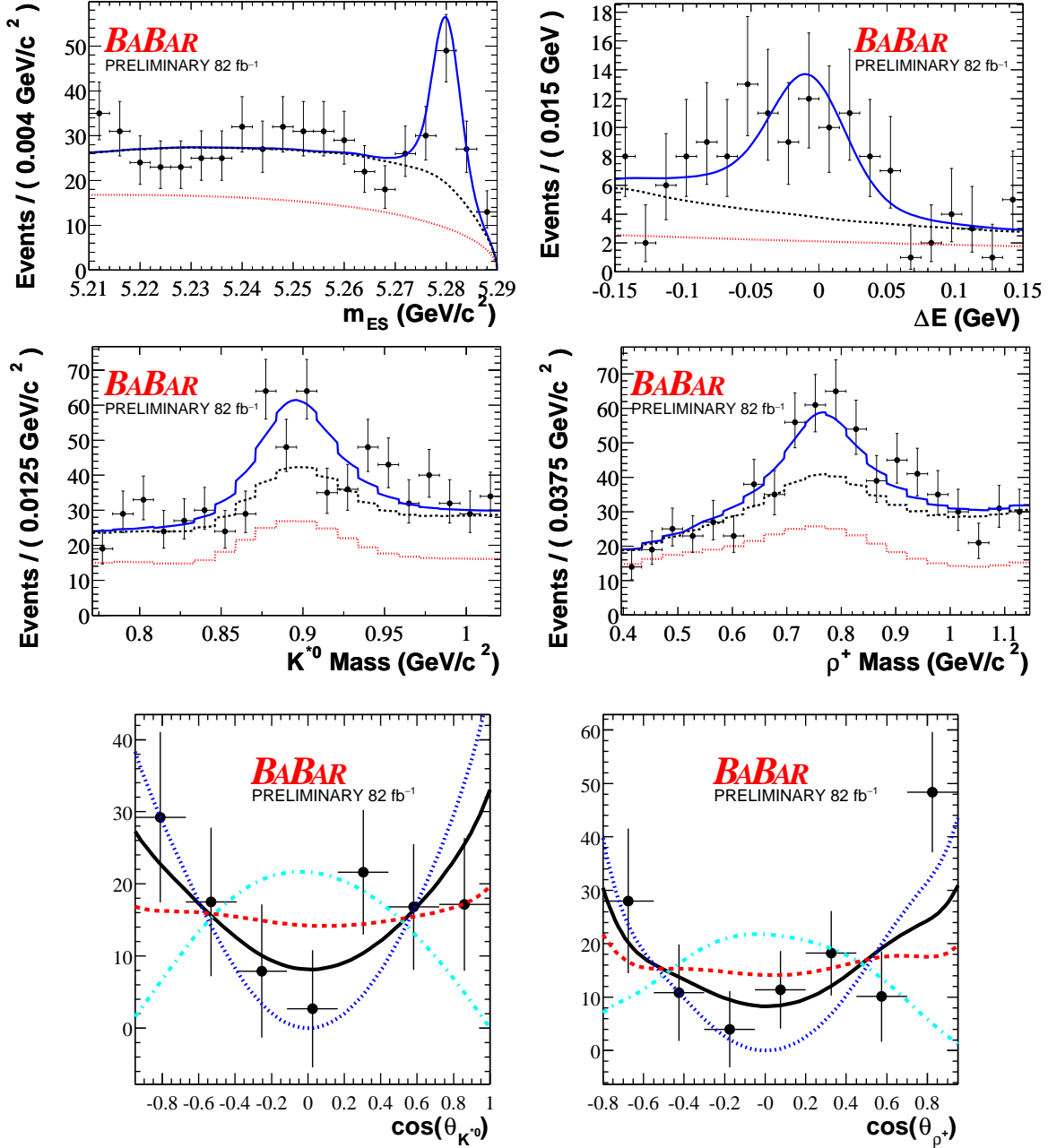
Figure 3: Distributions of m_{ES}, ΔE, K^{*0} and ρ^+ reconstructed masses and helicities in the $B^+ \to K^{*0}\rho^+$ decay, enhanced in signal component by selecting events with large signal to background likelihood ratios on the discriminating variables not shown in each plot. In the top four plots, the black dots are the data, the blue plain line is the fitted distribution for the full data sample, the black dashed line is the fitted distribution for all backgrounds, and the dotted red line is the distribution of only the continuum events. The two plots in the bottom show the distributions of the helicity angles. The data (black dots), after subtraction of the backgrounds, are compared to the signal component of the fitted PDF (plain black curve). In dashed lines are the results expected for different fractions of longitudinal component: 100% (blue), 50% (red), 0% (cyan). The pure transverse case is excluded by the data.

References

[1] A. Buras, R. Fleischer, S. Recksiegel, and F. Schwab. Anatomy of prominent B and K decays and signatures of CP–violating new physics in the electroweak penguin sector. (2004). hep-ph/0402112.

[2] M. Neubert and J.L. Rosner. Determination of the weak phase γ from rate measurements in $B^{\pm} \to \pi K, \pi\pi$ decays. *Phys. Rev. Lett.*, **81**:5076–5079, (1998). hep-ph/9809311.

[3] B. Aubert *et al.* [BABAR Collaboration]. Rates, polarizations, and asymmetries in charmless vector–vector B meson decays. *Phys. Rev. Lett.*, **91**:171802, (2003). hep-ex/0307026.

[4] J. Zhang *et al.* [BELLE Collaboration]. Observation of $B^{+} \to \rho^{+}\rho^{0}$. *Phys. Rev. Lett.*, **91**:221801, (2003). hep-ex/0306007.

[5] B. Aubert *et al.* [BABAR Collaboration]. Search for the decay $B^{0} \to K^{*+}\rho^{-}$. (2004). BABAR-CONF-04/041, SLAC-PUB-10636, hep-ex/0408035.

[6] A. Ali, G. Kramer, and Cai-Dian Lu. Experimental tests of factorization in charmless non-leptonic two-body B decays. *Phys. Rev.*, D**58**:094009, (1998). hep-ph/9804363.

[7] R. Aleksan, P. F. Giraud, V. Morenas, O. Pene, and A. S. Safir. Testing QCD factorization and charming penguins in charmless $B \to PV$. *Phys. Rev.*, D**67**:094019, (2003). hep-ph/0301165.

[8] A. Kagan. Polarization in $B \to VV$ decays. (2004). hep-ph/0405134, submitted to Phys. Lett. B.

[9] B. Aubert *et al.* [BABAR Collaboration]. Observation of the decay $B^{0} \to \rho^{+}\rho^{-}$ and measurement of the branching fraction and polarization. *Phys. Rev.*, D**69**:031102, (2004). hep-ex/0311017.

[10] B. Aubert *et al.* [BABAR Collaboration]. Measurement of the $B^{0} \to \phi K^{*0}$ decay amplitude. (2004). BABAR-PUB-04/031.

[11] A. Bosek *et al.* [BELLE Collaboration]. *Phys. Rev. Lett.*, **91**:201801, (2003). hep-ex/0307014.

[12] Y. Grossman. *Int. J. Mod. Phys.*, A**19**:907, (2004).

[13] P. Colangelo, F. De Fazio, and T. N. Pham. The riddle of polarization in $B \to VV$ transitions. (2004). hep-ph/0406162.

[14] G. Schott. Study of the rare decays $B \to K^{*}\rho/\rho\rho$ and search for CP violation in these modes in the *BABAR* experiment. Ph.D. Thesis, Paris 6 University, July (2004).

[15] G. Kramer and W.F. Palmer. *Phys. Rev.*, D**45**:193, (1992).

[16] B. Aubert *et al.* [BABAR Collaboration]. *Nucl. Instrum. Methods*, A**479**:1–116, (2002).

[17] S. Agostinelli *et al.* [GEANT4 Collaboration]. *Nucl. Instrum. Methods*, A**506**:250, (2003).

[18] B. Aubert *et al.* [BABAR Collaboration]. *Phys. Rev. Lett.*, **89**:281802, (2002).

[19] H. Albrecht *et al.* [ARGUS Collaboration]. *Z. Phys.*, C**48**:543, (1990).

[20] B. Aubert *et al.* [BABAR Collaboration]. Measurements of the branching fractions of charged B decays to $K^{\pm}\pi^{\mp}\pi^{\pm}$ final states. (2003). hep-ex/0308065, Submitted to Phys. Rev. D.